PHYSICAL REVIEW B

CONDENSED MATTER

THIRD SERIES, VOLUME 38, NUMBER 3 15 JULY 1988-II

Magnetism in bcc 3*d* transition metals: Onset and approach to the Hund's-rule limit

V. L. Moruzzi and P. M. Marcus

IBM Thomas J. Watson Research Center, Yorktown Heights, New York 10598

(Received 16 February 1988)

First-principles total-energy band theory is used to study the onset and the large-volume limit of magnetic behavior for the 3*d* transition metals constrained to the bcc crystal structure. It is found that all 3*d* transition metals from Sc to Ni undergo second-order, first-order, or composite second- and first-order transitions from nonmagnetic to magnetic behavior with increasing volume. An approximate Stoner analysis is used to interpret the structure of the transitions. As a function of volume, calculated magnetic moments generally increase and tend toward the free-atom limit in the local-spin-density approximation, and are consistent with Hund's rule. Calculated *d*-band widths vary as r^{-5} over a wide range of volumes, in agreement with Heine's theoretical results.

I. INTRODUCTION

We have previously shown that transition metals exhibit a range of magnetic properties when examined as a function of volume. Normally magnetic transition metals can be rendered nonmagnetic at compressed volumes and normally nonmagnetic transition metals can be rendered ferromagnetic at expanded volumes. It is expected that all transition metals must undergo transitions from nonmagnetic to magnetic behavior as the volume is increased, and, in the limit of large volumes, the magnetic moment must approach a value consistent with Hund's rule and the free-atom ground-state configuration. Self-consistent energy-band calculations demonstrate that these magnetic transitions are characterized by calculated magnetic moments which exhibit singular[1,2] behavior at well-defined critical values of volume. Different types of magnetic behavior, classified as nonmagnetic (NM), low-spin (LS), or high-spin (HS), and different transition types, classified as type I, type II, type III, etc. depending on the number (one, two, three, etc.) of critical points displayed, have been found. These transitions, in turn, are identified as second-order (type I), first-order (type II), and composite second-order and first-order (type III, etc.) transitions, depending upon the details of calculated total energy versus volume curves.

In previous work,[3,4] we have shown that bcc V, Cr, Mn, and Fe undergo type-III, -II, -III, and -I magnetic transitions, respectively, at certain critical volumes. The present work is an extension of this earlier work and includes the light transition metals Sc and Ti, and the heavy transition metals Co and Ni; thereby completing the series from Sc to Ni. In the present work, we show that all 3*d* transition metals exhibit magnetic properties and also study the approach to the free-atom limit. We restrict ourselves to the 3*d* series constrained to the bcc structure, and consider only nonmagnetic or ferromagnetic (parallel-spin-moment) states. In the large-volume limit, these structural and magnetic constraints become increasingly less important and the system attains the free-atom character.

Our work is based on self-consistent parameter-free total-energy band calculations and utilizes the augmented-spherical-wave method[5] and the fixed-spin-moment procedure[6] to calculate the magnetic moment, M, as a function of volume, V, or equivalently, as a function of the Wigner-Seitz radius, r_{WS}, where $V=\frac{4}{3}\pi r_{\mathrm{WS}}^3$. The local-spin-density approximation (LSD) is used for exchange and correlation. This approximation is expected to be more valid for condensed systems than for inhomogeneous systems like free atoms.

Our present work can be divided into two parts. In Sec. II, we study the onset of magnetic behavior. We present new results for the volume dependence of the magnetic moment and the total energies for Sc, Ti, Co, and Ni, and review our published results for V, Cr, Mn, and Fe. We also use an approximate Stoner analysis to interpret the structure of the magnetic transitions, and show that three types of density-of-states (DOS) curves can explain the three types of transitions found for the series. In Sec. III, we study the large-volume limiting behavior of the magnetic moment and show that the moment approaches the free-atom limit dictated by Hund's rule and the ground-state atomic configuration.

II. ONSET OF MAGNETISM

Calculated magnetic moments and total energies for the light transition metals Sc and Ti are shown in Figs. 1

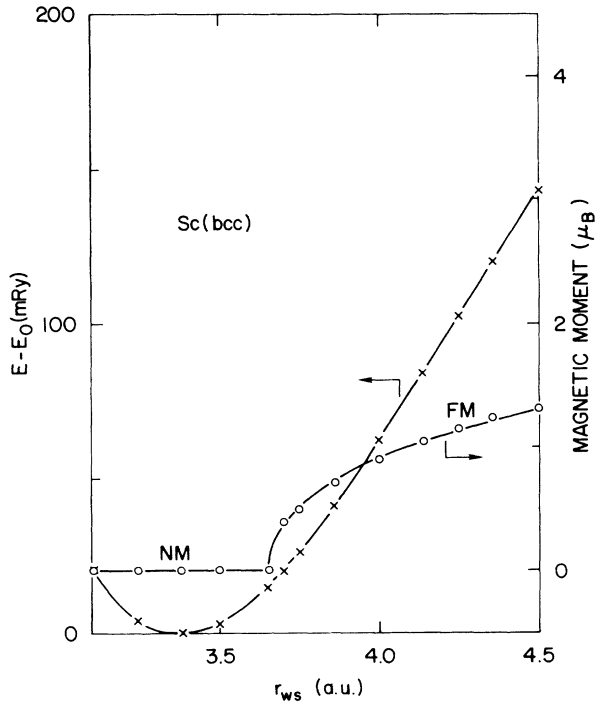

FIG. 1. Calculated magnetic moment and total energy as a function of r_{WS} for bcc Sc, showing a type-I second-order transition from a nonmagnetic (NM) to a ferromagnetic (FM) state.

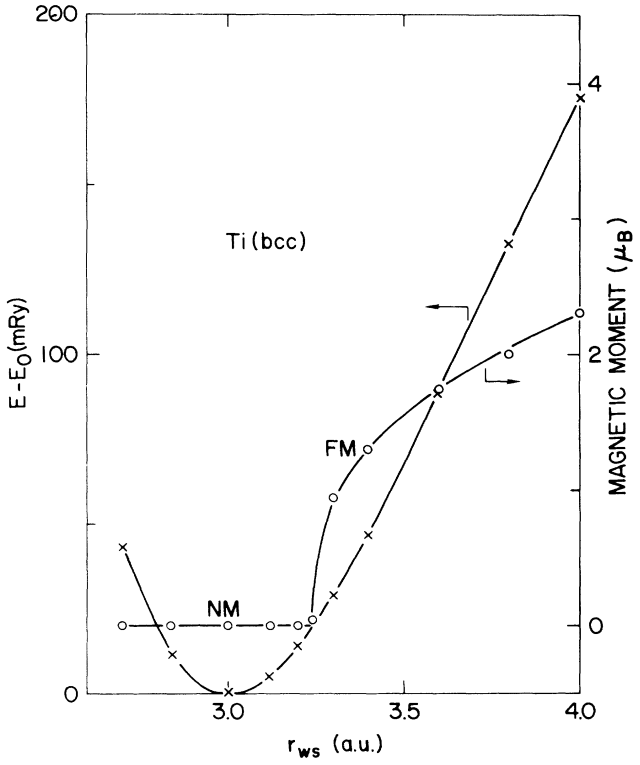

FIG. 2. Calculated magnetic moment and total energy as a function of r_{WS} for bcc Ti, showing a type-I second-order transition from a nonmagnetic to a ferromagnetic state.

and 2, respectively. Although these metals, which are actually hexagonal, are not normally considered to be magnetic, we see that they undergo second-order transitions from nonmagnetic to magnetic behavior at critical volumes slightly larger than the indicated equilibrium volumes. We note that the Hund's-rule free-atom moments for the experimental ground-state configurations ($1\mu_B$ and $2\mu_B$, respectively for these two systems) are exceeded. The bulk moduli, B, obtained from the curvatures of the energy versus r_{WS} curves, commonly called binding curves, are 530 and 1000 kbar, respectively.

The moments and total energies for V, Cr, Mn, and Fe are given in Ref. 3. V and Mn undergo composite second-order and first-order transitions, Cr undergoes a first-order transition, and Fe undergoes a second-order transition similar to Sc and Ti. The first-order transition for Cr is at expanded volumes, while the second-order transition for Fe is at compressed volumes.

Our results for Co and Ni are shown in Figs. 3 and 4, respectively. Co, which is normally magnetic, is nonmagnetic at compressed volumes where a second-order transition occurs. For Ni, we find a second-order transition near the equilibrium volume. The calculated bulk moduli are 2300 and 2100 kbar, respectively.

Table I summarizes the results of this study and shows that transition metals can exhibit a wide range of magnetic properties when examined as a function of volume. The listed critical r_{WS} values define the ranges for the different types of behavior. In all cases, the NM critical value refers to the termination or stability limit of NM

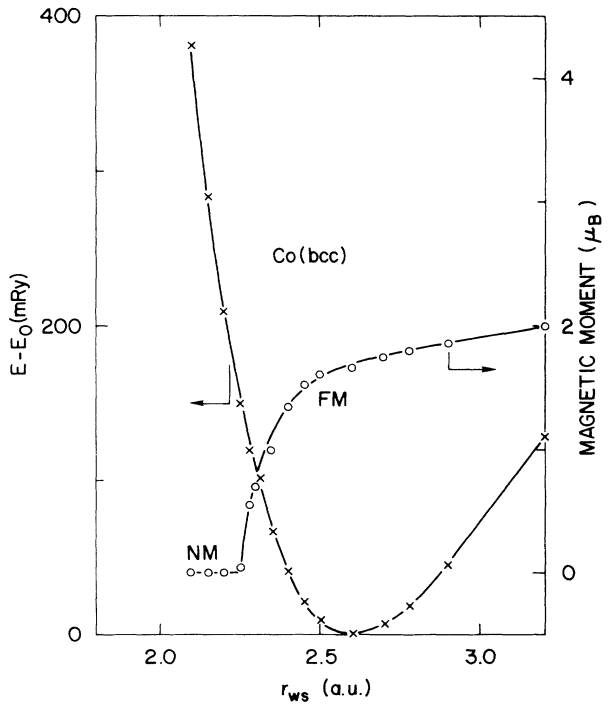

FIG. 3. Calculated magnetic moment and total energy as a function of r_{WS} for bcc Co, showing a type-I second-order transition from a nonmagnetic to a ferromagnetic state.

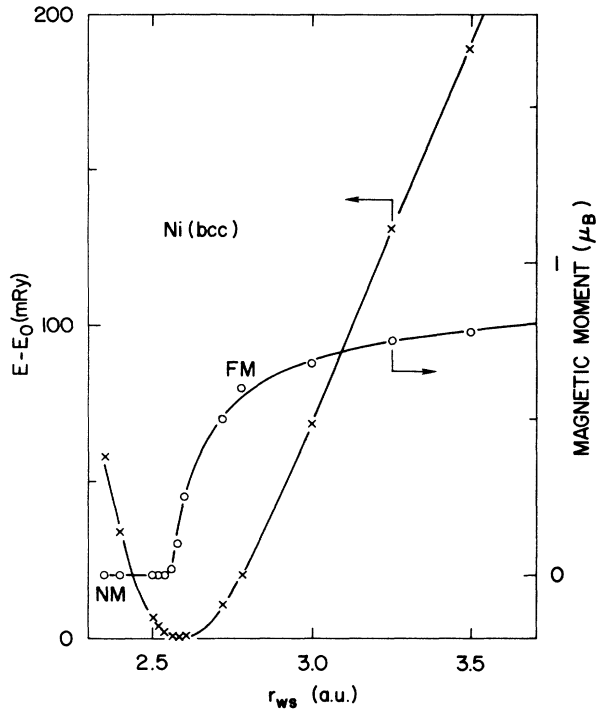

FIG. 4. Calculated magnetic moment and total energy as a function of r_{WS} for bcc Ni, showing a type-I second-order transition from a nonmagnetic to a ferromagnetic state.

behavior, and the HS critical value refers to the beginning or stability limit of HS or FM (ferromagnetic) behavior. V and Mn, which have type-III transitions, exhibit LS behavior in the region between the indicated critical r_{WS} values. For Sc, Ti, Fe, Co, and Ni, which show type-I or second-order transitions, the termination of NM behavior coincides with the beginning of HS behavior and the binding curves are continuous. Here, the terms high-spin and ferromagnetic both refer to magnetic behavior that persists to large volumes.

Our self-consistent, fixed-spin-moment calculations show that, in this series, the transitions from nonmagnetic to magnetic behavior are second order, first order, or composite second and first order. Although these calculations stand alone, it is interesting to note that a Stoner analysis, particularly in the form developed by Andersen *et al.*,[7] can provide a useful understanding of the onset of magnetic behavior and of the differences in the form of the transitions. At a given r_{WS} value, the Stoner criterion can be expressed in the form

$$\bar{N}(M)I = 1 ,$$

where $\bar{N}(M)$ is DOS averaged over an energy interval spanning the range corresponding to $M/2$ states in the majority band above the Fermi energy (E_F), and $M/2$ states in the minority band below E_F. Here, the majority and minority bands are constructed from a DOS derived from non-spin-polarized band calculations, with rigid shifts of the up-spin and down-spin bands with respect to the nonmagnetic E_F leading to a magnetic moment M. The Stoner exchange parameter, I, is a system-specific coefficient of an effective exchange-correlation field that lowers the total energy of the system by $M^2I/4$. Magnetic behavior is favored at expanded volumes because $N(E_F)$ grows rapidly as the bands become narrower (the d-band width varies as r_{WS}^{-5}) with increasing volume. As a consequence, $\bar{N}(M)$ also increases until the Stoner criterion is exceeded. The functional form of $\bar{N}(M)$ depends on the detailed position of E_F in the DOS (i.e., whether it falls in a deep minimum or in a peak), and determines the order of the transition. In Fig. 5, we show schematic representations of the $\bar{N}(M)$ behavior for the systems studied here. In all cases, volume increases towards the top of each panel. Curves labeled V_{NM} show the expected functional dependence at compressed volumes where nonmagnetic behavior is preferred and curves labeled V_T show the dependence at or near the calculated critical points. Curves labeled V_{HS} or V_{FM} show the dependence at expanded volumes where high-spin or ferromagnetic behavior is preferred. The solid horizontal bars at $1/I$ indicate the range of allowed magnetic moments, and are labeled HS, FM, or LS in accordance with the labeling in Figs. 1–4 and Refs. 1 and 2. The vertical lines represent the expected limiting free-atom behavior discussed in Sec. III.

TABLE I. Equilibrium Wigner-Seitz radii (a.u.), ground states, bulk moduli (kbar), transition types, and critical Wigner-Seitz radii (a.u.) for the 3d transition metals constrained to the bcc structure. The NM critical r_{WS} value refers to the termination of NM behavior, and the HS critical value refers to the beginning of HS or FM behavior. Systems which have type-III transitions exhibit LS behavior in the region bounded by the indicated LS critical r_{WS} values.

System	r_{WS} (equil.)	Ground state	Bulk modulus	Transition type	Critical r_{WS} values NM	LS	HS
bcc Sc	3.36	NM	530	I	3.65		3.65
bcc Ti	3.01	NM	1000	I	3.24		3.24
bcc V	2.79	NM	1800	III	3.17	3.17,3.53	3.47
bcc Cr	2.59	NM	2700	II	3.46		3.12
bcc Mn	2.59	LS	2600	III	2.53	2.53,2.92	2.88
bcc Fe	2.62	FM	2200	I	2.28		2.28
bcc Co	2.60	FM	2300	I	2.26		2.26
bcc Ni	2.60	FM	2100	I	2.56		2.56

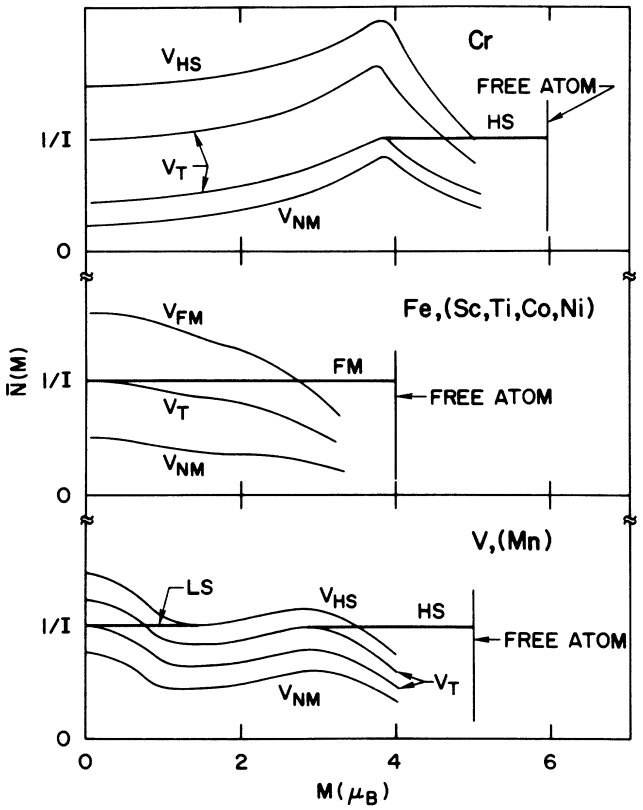

FIG. 5. Schematic behavior of $\bar{N}(M)$ for the bcc $3d$ transition metals at different volumes, showing the Stoner analysis leading to first-order (top panel), second-order (middle panel), and composite (bottom panel) transitions. The top panel represents the behavior for bcc Cr, the middle panel represents the behavior for bcc Fe (as well as Sc, Ti, Co, and Ni), and the lower panel represents the behavior for bcc V (and Mn).

In the nonmagnetic state, the DOS for the bcc systems included in this study show three peaks capable of accommodating approximately 2, 4, and 6 (s plus d) electrons, respectively.[8] Going across the $3d$ transition series Sc has three valence electrons, and the number increases by one with each increase in atomic number, reaching ten for Ni. By adopting such a three-peaked canonical DOS for the entire series, the extra electrons are accommodated by simply moving E_F to higher energies to occupy successively more states as a function of increasing atomic number. In the process, E_F falls on successively higher peaks, or in deep minima between peaks. Each half of the spin-split DOS shows the same three-peaked structure, with half as many electrons (i.e., 1, 2, and 3).

For nonmagnetic bcc Cr, which has six valence electrons, E_F falls in the deep minimum between the two uppermost peaks in the DOS.[8] As shown in the top panel of Fig. 5 $\bar{N}(M)$ must therefore have a positive curvature at the origin and must rise to a peak at a finite M value near $4\mu_B$, corresponding to positioning E_F in the uppermost peak of the majority bands with approximately five up spins and in a local minimum in the minority bands with approximately one down spin. As r_{WS} increases, the entire $\bar{N}(M)$ curve increases. At some critical value of r_{WS}, the peak at $M \simeq 4\mu_B$ reaches the value $1/I$ and satisfies the Stoner criterion. The system therefore goes magnetic with a discontinuous jump to $M \simeq 4\mu_B$. With still larger increases in r_{WS}, M simply continues to rise to the free-atom limit. Thus, Cr undergoes a first-order transition and exhibits a gap in the allowed magnetic moments, with no solutions between $M=0$ and $M \simeq 4\mu_B$.

The middle panel of Fig. 5 represents the situation for Fe. In this case, there are eight valence electrons to account for and E_F falls on the uppermost peak in the DOS.[8] Since E_F falls on a peak, $\bar{N}(M)$ at $M=0$ is large, but decreases with increasing M, with E_F above the peak for the majority bands and below the peak for the minority bands, resulting in a negative curvature. At low volumes, $\bar{N}(M)$ does not exceed the Stoner criterion and the system is nonmagnetic. As the volume increases, $\bar{N}(M)$ increases until it exceeds $1/I$ at some critical r_{WS} value at $M=0$. The system then goes magnetic, and further increases in volume simply increase M in a smooth manner. Thus Fe undergoes a second-order transition with M varying smoothly from zero to the free-atom limit. For bcc, Sc, Ti, Co, and Ni, E_F falls in or near a local peak in the nonmagnetic DOS and the systems show similar (second-order) transitions.

Finally, consider V with five valence electrons and E_F just to the right of the central DOS peak.[8] In this case, $\bar{N}(M)$ has a somewhat more complicated form. As shown in the lower panel of Fig. 5, $\bar{N}(M)$ now has two peaks, one at $M=0$, and one near $M=3\mu_B$. This second peak is a consequence of positioning E_F in the uppermost peak of the majority bands with approximately four up spins, and in a local minimum in the minority bands with approximately one down spin. The schematic curves show the behavior as the volume is increased. At some critical r_{WS} value, $1/I$ is exceeded and the system undergoes a second-order transition (similar to Fe) from nonmagnetic behavior to LS behavior. Increasing r_{WS} simply increases the moment until a second critical r_{WS} value is reached. Here, the system can have two values of magnetic moment, the LS value, and a second HS value at $M \simeq 3\mu_B$. As the volume is increased further, the LS solution ends at a third critical r_{WS} value, but the HS moment persists up to the free-atom value. Thus V (and similarly Mn) undergoes a composite transition, beginning with a second-order and ending with a first-order transition.

We see that the functional form of $\bar{N}(M)$ depends upon details of the nonmagnetic DOS and upon the location of E_F. In general, if E_F falls in a deep minimum of the nonmagnetic DOS, $\bar{N}(M)$ will have a positive curvature at the origin (the slope must be zero because of $\pm M$ symmetry). $\bar{N}(M)$ will peak at a finite M value with E_F on a local peak in the spin-split bands, and the system will undergo a first-order transition. On the other hand, if E_F falls on a peak in the nonmagnetic DOS, $\bar{N}(M)$ will have a negative curvature at the origin and the system will undergo a second-order transition. As the functional form of $\bar{N}(M)$ becomes more complicated due to details of the DOS, still more complicated transitions can occur. Thus fcc Fe was shown[1,2] to exhibit two first-order transitions

in a very limited volume range. A recent Stoner analysis by Krasko[9] confirmed this complicated behavior.

III. LARGE-VOLUME LIMIT

In 3*d* transition-metal atoms, the uppermost occupied energy levels correspond to 3*d* and 4*s* states. Upon condensation, these levels broaden and overlap to form conduction bands leading to a DOS with mixed *sp* and *d* states. At the zero-pressure equilibrium volume, the 3*d* and 4*s* bands are partially occupied with E_F in the *d* bands. This mixing of *sp* and *d* states in solids is apparent in non-spin-polarized energy-band calculations which, for both bcc and fcc 3*d* transition metals, yield approximately 1.4 *sp* electrons. Thus, at equilibrium, $n_{sp} \simeq 1.4$ electrons, regardless of the atomic ground-state configuration. The number of *d* electrons, n_d, is 1.6 for Sc, increases by 1 with successive increases in atomic number, and finally reaches 8.6 for Ni. Therefore, the familiar integer atomic configuration values do not apply for condensed systems.

In general, the zero-pressure equilibrium state is not a state of maximum spin. That is, Hund's rule is not satisfied and the magnetic moment does not have its maximum value. However, as the volume increases, the bands become narrow and approach the discrete levels of a free atom and Hund's rule for the ground-state configuration is satisfied. In order to study this experimentally inaccessible but theoretically interesting limit, we have extended the volume range and calculated magnetic moments out to $r_{WS} \simeq 6$ a.u. (7 a.u. for Sc). The magnetic behavior deduced from a study of calculated $E(M)$ curves is shown in Fig. 6, where ↓'s indicate equilibrium r_{WS} points. Spin moments consistent with Hund's rule and experimental ground-state atomic configurations are also shown.

Figure 6 shows that the limiting atomic configuration is not always the experimental free-atom configuration, but that it corresponds rather to the ground-state configuration of an atom calculated[10] in the LSD approximation. The ground-state configurations and resulting magnetic moments of the LSD atom are different from those of the experimental free atom for Ti and V. Here, the LSD atoms have a single 4*s* electron while the experimental atoms have two 4*s* electrons (a $4s^2$ configuration) and a smaller moment. The LSD atom satisfies Hund's rule, but by transferring an electron from the *s* to the *d* shell, Hund's rule is applied to *two* unfilled shells and results in a larger moment. The LSD and experimental atom have the same magnetic moment for all systems except Ti and V.

A striking feature in Fig. 6 is the manner in which the magnetic moment approaches the Hund's-rule limit. The moment approaches its limiting value at large volumes with a steep slope from below for all systems except Sc which has a steep slope from above. We find that the limiting moment is attained at a definite volume where the *s* bands separate from the *d* bands, fall below E_F, and become fully occupied. At this volume, there is a discontinuity in the slope of M that is a consequence of an infinite slope at the termination of the *s*-band DOS.

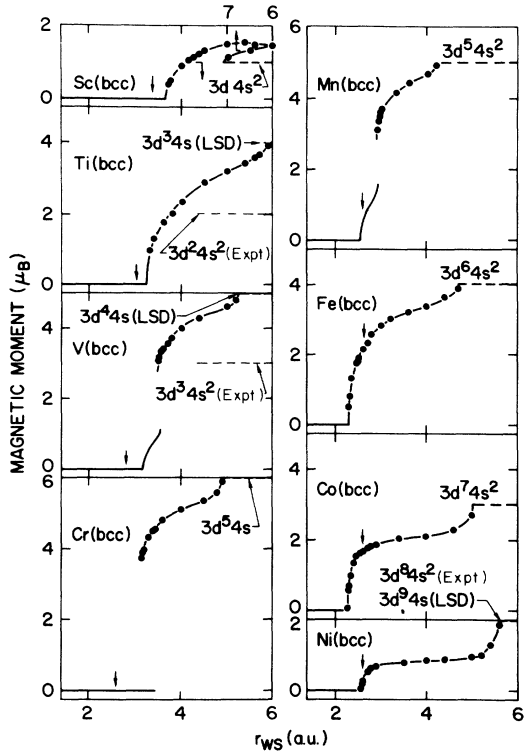

FIG. 6. Calculated magnetic moments for the 3*d* transition elements constrained to the bcc structure showing the large-volume limit and the approach to the Hund's-rule atomic limit. Only calculated points in the ferromagnetic or high-spin region are shown.

In the case of Sc, the LSD atom and the experimental atom have the same ground-state configuration, but before reaching the limiting behavior, the 4*s* shell is partially filled and polarized. At larger r_{WS} values, the moment decreases to the Hund's-rule value of $1\mu_B$ with a discontinuous slope near $r_{WS} = 7$ a.u. (note, the r_{WS} axis is folded back in Fig. 6 to display the curve out to larger radii). For Sc at large volume, E_F is pinned in a deep minimum in the majority *d* band, and the minority *d* band is unoccupied.

Figure 7 shows the spin-split DOS for bcc Fe at $r_{WS} = 4.70$ a.u. where the calculated magnetic moment is $3.9\mu_B$. For this point, we find 0.92 $sp^{\uparrow}$, 5.02 $d^{\uparrow}$, 0.53 $sp^{\downarrow}$, and 1.52 $d^{\downarrow}$ electrons so that the effective configuration is $3d^{6.54}4s^{1.45}$. Note that this configuration approaches the $3d^{6.4}4s^{1.6}$ configuration found for the LSD atom.[10] Figure 7 demonstrates that even at this volume, where the majority and minority *d* bands are approaching atomic-like energy levels, the bands still retain the same general shape of the bcc bands at equilibrium volumes. Thus the bcc signature of the lattice is still apparent at these large volumes. Note also that E_F is pinned in the deep minimum in the minority *d* bands, and that the *sp* bands are still spread over a wide energy range.

Analysis of a series of DOS for Fe in the range from the equilibrium r_{WS} value to $r_{WS} = 4.70$ a.u. where Hund's rule is approached, yields a mapping of the *d*-

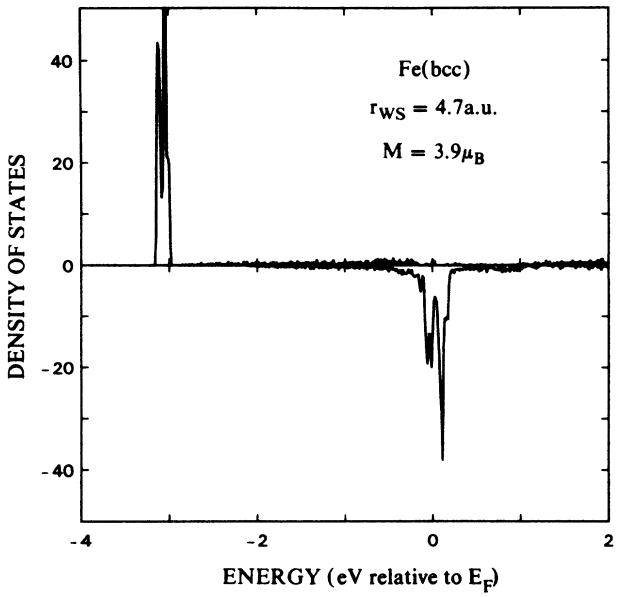

FIG. 7. DOS in states/eV unit-cell for bcc Fe at $r_{WS}=4.7$ a.u. where $M=3.9\mu_B$.

band edges (defined by the steep fall where they merge into the s bands) shown in Fig. 8. We see that the d bands overlap for $r_{WS} < \simeq 3$ a.u. For larger radii, the d bands separate and the subsequent increase in magnetic moment corresponds first to further d-band polarization and later to s-band polarization. The calculated energy-level splitting for the LSD free atom in a $3d^{6.5}4s^{1.5}$ configuration is 225 mRy and shown[11] at $r_{WS}=\infty$. As shown in Fig. 7, the sp bands are spread in energy and difficult to resolve. The majority and minority Fe d-band

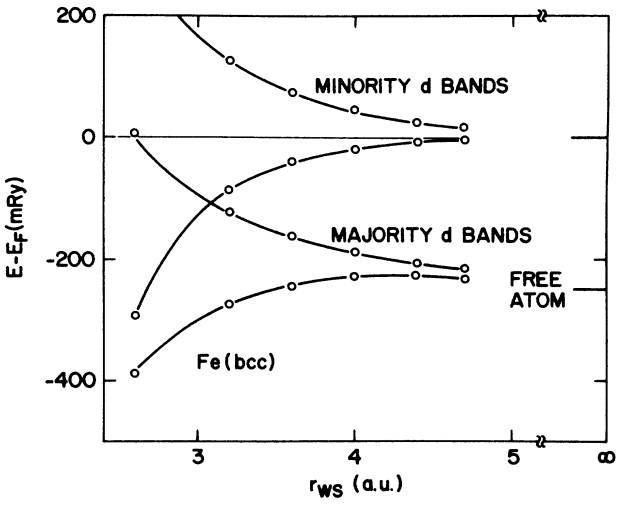

FIG. 8. Calculated d bands for bcc Fe showing the approach to the free-atom limit. The effective configuration at $r_{WS}=4.70$ a.u. is $3d^{6.54}4s^{1.45}$. The d-level separation for the LSD free atom in the $3d^{6.5}4s^{1.5}$ is indicated at $r_{WS}=\infty$.

widths, plotted as a function of r^{-5} are shown in Fig. 9. The linear behavior displayed is a direct (computational) verification, over a wide range of r_{WS} values, of Heine's r^{-5} dependence for d-band widths.[12] The majority d band is lower in energy than the minority d band, and consequently is systematically narrower. Note that the data do not extrapolate to zero, because the d bands are imbedded in the sp bands and the edges are not precisely defined. As the widths increase beyond the range shown in Fig. 9, the uncertainties become more important, and deviations from linearity are expected because the two bands must eventually merge into one (have the same width) at $r_{WS}=2.28$ a.u. where the system becomes nonmagnetic.

In Table II, we list calculated spin configurations at the indicated r_{WS} values where the s bands separate from the d bands. Note that the LSD free-atom limit is not attained even at these large volumes because we are still in a region where majority and minority sp bands overlap. From the table, it is apparent that atomic configurations are approached but not completely reached at these r_{WS} values. The full atomic configuration can be achieved, for the most part, by electron transfer: from the majority d band to the minority sp band for Sc, from the majority and the minority sp bands to the majority d band for Ti, from the minority sp band to the majority sp band for V,

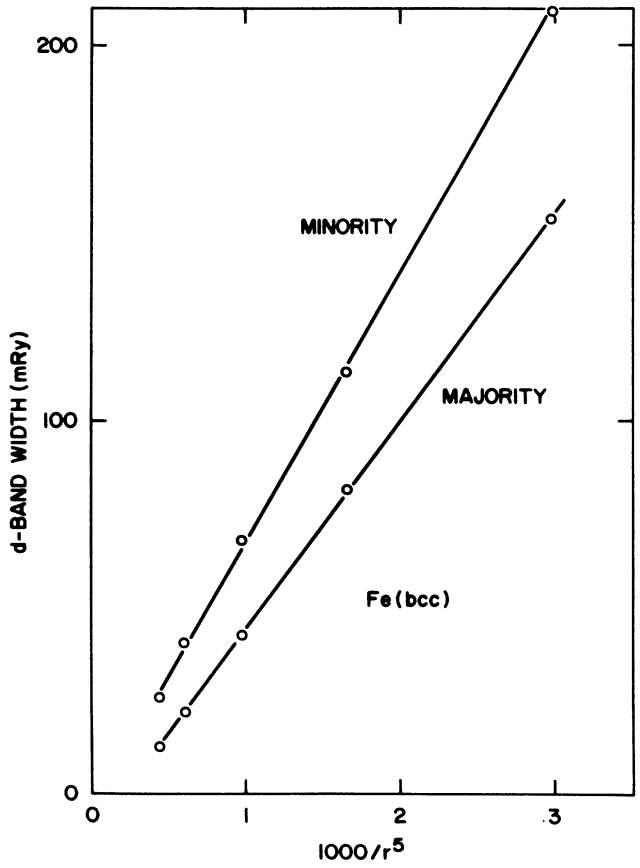

FIG. 9. Band widths for majority and minority d bands for bcc Fe showing Heine's r^{-5} dependence.

TABLE II. Approximate spin configurations at the indicated radii (a.u.) and magnetic moments (μ_B) for the 3d transition metals constrained to the bcc structure. The configurations are appropriate to the systems at large volumes near the radius where the sp and d bands separate. Larger volumes are necessary to achieve the "full" LSD atomic configurations.

			Majority		Minority		
System	r_{WS}	M	$sp^{\uparrow}$	$d^{\uparrow}$	$sp^{\downarrow}$	$d^{\downarrow}$	Config.
bcc Sc	7.00	1.10	0.97	1.08	0.92	0.03	$3d^{1.11}4s^{1.89}$
bcc Ti	5.90	3.90	1.06	2.89	0.04	0.01	$3d^{2.90}4s^{1.10}$
bcc V	5.20	4.80	0.90	4.00	0.10	0.00	$3d^{4.00}4s^{1.00}$
bcc Cr	4.90	5.90	1.00	4.95	0.05	0.00	$3d^{4.95}4s^{1.05}$
bcc Mn	4.20	4.95	0.94	5.01	0.65	0.40	$3d^{5.41}4s^{1.59}$
bcc Fe	4.70	3.90	0.92	5.02	0.53	1.52	$3d^{6.54}4s^{1.45}$
bcc Co	5.00	2.70	0.84	5.01	0.39	2.76	$3d^{7.77}4s^{1.23}$
bcc Ni	5.60	1.87	0.93	5.01	0.09	3.97	$3d^{8.98}4s^{1.02}$

from the minority sp band to the majority d band for Cr, from the minority d band to the minority sp band for Mn and for Fe and Co. For Ni, the atomic configuration can be reached by electron transfer from the minority to the majority sp bands.

IV. DISCUSSION

Both Fig. 6 and Table I show interesting trends across the 3d transition series. With increasing atomic number, the equilibrium r_{WS} values decrease rapidly and become relatively constant from Cr through Ni. This same trend is apparent in the r_{WS} values corresponding to the location where the s bands separate from the d bands (Fig. 6 or Table II). In fact, the ratio of this latter quantity to r_{WS} at equilibrium is approximately constant and equal to 2 for all members of the series. The bulk moduli increase rapidly, reach a maximum at Cr and then drop slightly, and become relatively constant for Fe, Co, and Ni. It is interesting to note that although many of the systems considered do not occur in nature (the 3d transition metals do not all have bcc ground-state structures), the trends are in general agreement[8] with experimental trends in real systems. The bulk modulus for Mn seems to be the one exception, with the experimental value being much lower than our calculated value. This may be due to the fact that the ground state of naturally occurring Mn is antiferromagnetic.

We note that, for the bcc structure, the magnetic transitions are second-order for the light and heavy transition metals, and first-order or composite for the middle transition metals. This is a direct consequence of the position of E_F, and the three-peaked bcc DOS, as discussed in the Stoner analysis given in Sec. II.

In the large-volume limit, the majority d bands for Cr, Mn, Fe, Co, and Ni are completely filled (five electrons), as shown in Table II and demonstrated graphically for Fe in Figs. 7 and 8. For these systems, E_F is pinned in a deep minimum in the *minority* d bands. For Sc, Ti, and V, Table II shows that the minority d bands are empty. For these systems, E_F is pinned in a deep minimum in the *majority* d bands. Ti, V, and Cr tend towards a $4s^1$ configuration and have increased magnetic moments due to s-electron polarization. In the case of Sc, the magnetic moment is initially enhanced due to s-electron polarization, but in this case the moment drops off at larger volumes and approaches a $3d4s^2$ configuration from above with a moment of $1\mu_B$. Cr is a special case and has the largest moment because of the fully occupied majority, and completely empty minority d and sp bands.

The calculated magnetic moments display yet another trend in the 3d transition series. In Fig. 10, we show the LSD free-atom moments (integers) along with the experimental magnetic moments for Fe, Co, and Ni which fall on the familiar Slater-Pauling (SP) curve. The SP curve shows the saturation moment due to an applied field at the equilibrium (zero-pressure) volume, as a function of

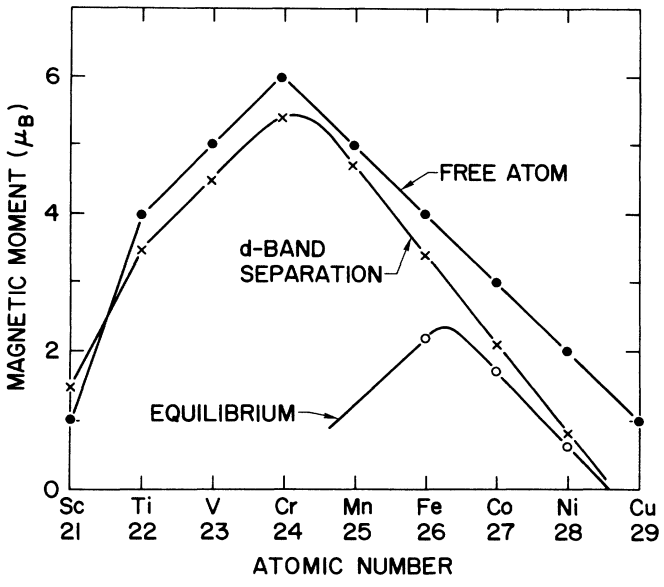

FIG. 10. Saturation moments for the 3d transition metals. The "equilibrium" curve is the familiar Slater-Pauling curve for the metals. The "free-atom" curve gives the maximum moment for the LSD atom and represents the total exchange-saturated moments from both s and d states. The "d-band separation" curve gives the exchange-saturated moments at d-band separation, or at volumes where the minority d bands are completely empty (zero electrons, light transition metals) or where the majority d bands are full (five electrons, heavy transition metals).

atomic number. Our calculated large-volume magnetic moments represent the saturation moments for the exchange-correlation field. The effects of this exchange-correlation field are progressively enhanced by increasing the volume and result in an exchange-saturated moment that measures the ultimate magnetic capability of the system. Our LSD free-atom SP curve differs from the usual SP curve by giving larger moments, by including Sc, Ti, V, and Cr, and by peaking at Cr instead of Fe. We also show in Fig. 10, the magnetic moments at "*d*-band separation." This calculated magnetic moment is obtained from the inflection points of the curves in Fig. 6 (except for Sc, where the maximum is used), and gives the moment at volumes where the minority *d* bands are approximately empty for the light transition metals, and volumes where the majority *d* bands are approximately full for the heavy transition metals.[13] That is, for the light transition metals, the minority *d* bands are above E_F (empty), and for the heavy transition metals, the majority *d* bands are below E_F (full) and contain five electrons. From Cr to Ni, the additional *s*-state contribution to the moment beyond the inflection point becomes increasingly larger, as is evident from the differences between the free-atom and *d*-band separation curves. Cu, with a $3d^{10}4s$ ground-state configuration has a free-atom moment of $1\mu_B$ derived exclusively from *s* states.

Note that the curves in Fig. 6 show two stages of saturation. In the first stage, the curves show an initial rise and then round over to a plateau corresponding to the splitting of the majority and minority *d* bands (near $r_{WS} \simeq 3$ a.u. for Fe) in the exchange field (the *d*-band separation mentioned above). For the light transition metals, the plateau corresponds to approximately empty minority *d* bands (above E_F) with all the *d* electrons in majority *d* bands (below E_F). For the heavy transition metals, the plateau corresponds to approximately full (five electrons) majority *d* bands (below E_F). Thus, the plateau represents a region where we would observe no change in moment if there were only *d* electrons to deal with. However, the presence of *s* bands produces further changes as the majority and minority *s* bands become narrow and split with increasing volume. The trend curve in Fig. 10, labeled "*d*-band separation" represents an estimate of the plateau region.

In the light transition metals, the moment can rise above the plateau when the majority *s* band drops below E_F while the minority *s* band remains above E_F. Hence the moment is enhanced both by polarization of the *s* bands and by electron transfer to the majority *d* bands, producing the final saturation moment of the LSD atom. However, in the case of Sc, both majority and minority *s* bands become occupied (fall below E_F), and the moment is reduced from its value at the plateau before reaching full saturation.

In the heavy transition metals, the magnetic moment at *d*-band separation corresponds to almost fully polarized *d* bands, and unpolarized or slightly polarized *s* bands, each containing approximately $\frac{1}{2}$ electron. The final rise in magnetic moment when one or both *s* bands drop below E_F is achieved either by *s*-band transfer (one *s* band below E_F) and increased *s*-band polarization, or by *d*-band to *s*-band transfer (both *s* bands below E_F) and increased *d*-band polarization. However, the final moment is the same for Mn, Fe, Co, and Ni, whether one ($3d^x4s$) or both ($3d^{x-1}4s^2$) *s* bands fall below E_F.

In summary, we have used first-principles total-energy band calculations with the local-spin-density and spherical-atom approximations to study the volume dependence of the magnetic moments, and to identify volume regions of different magnetic behavior. We have obtained a complete and theoretically consistent description of the magnetic behavior at all volumes out to the free-atom limit. Although the physically accessible range of volumes is perhaps only a $\pm 10\%$ volume change around the equilibrium volume, and the large-volume limit lies far beyond the stability limit of the lattice (where the bulk modulus goes to zero), our results give a comprehensive description of the magnetic behavior and of the trends and electronic changes in the bcc 3*d* transition metals.

---

[1]V. L. Moruzzi, Phys. Rev. Lett. **57**, 2211 (1986).
[2]V. L. Moruzzi, P. M. Marcus, K. Schwarz, and P. Mohn, Phys. Rev. B **34**, 1784 (1986).
[3]V. L. Moruzzi, P. M. Marcus, and P. C. Pattnaik, Phys. Rev. B **37**, 8003 (1988).
[4]P. M. Marcus and V. L. Moruzzi, J. Appl. Phys. (to be published).
[5]A. R. Williams, J. Kübler, and C. D. Gelatt, Jr., Phys. Rev. B **19**, 6094 (1979).
[6]A. R. Williams, V. L. Moruzzi, J. Kübler, and K. Schwarz, Bull. Am. Phys. Soc. **29**, 278 (1984); K. Schwarz and P. Mohn, J. Phys. F **14**, 1129 (1984).
[7]O. K. Andersen, J. Madsen, U. K. Poulsen, O. Jepsen, and J. Kollar, Physica B + C **86-88B**, 249 (1977).
[8]V. L. Moruzzi, J. F. Janak, and A. R. Williams, *Calculated Electronic Properties of Metals* (Pergamon, New York, 1978).
[9]G. Krasko, Phys. Rev. B **36**, 8565 (1987).
[10]See page 8 of Ref. 8.
[11]J. F. Janak (private communication).
[12]V. Heine, Phys. Rev. **153**, 673 (1967).
[13]At *d*-band separation, the majority *d* bands are not completely full, and the minority *d* bands are not completely empty because the *s* and *d* bands still overlap and some residual *s*-*d* electron transfer can occur all the way up to the free-atom limit. We cannot make a precise statement about the filling of the *d* and *s* bands because, as in any band calculation, the states are mixed and are neither pure *d* nor pure *s*.